Role of Abnormally Enhanced MJO over the Western Pacific in the Formation and Subseasonal Predictability of the Record-breaking Northeast Asian Heatwave in the Summer of 2018

Pang-Chi Hsu[1], Yitian Qian[1, 2], Yu Liu[1, 4], Hiroyuki Murakami[2, 3], Yingxia Gao[1]

[1]Key Laboratory of Meteorological Disaster of Ministry of Education/Joint International Research Laboratory of Climate and Environment Change/Collaborative Innovation Center on Forecast and Evaluation of Meteorological Disasters, Nanjing University of Information Science & Technology, Nanjing, China

[2] National Oceanic and Atmospheric Administration/Geophysical Fluid Dynamics Laboratory, Princeton, NJ, USA

[3]University Corporation for Atmospheric Research, Boulder, CO, USA

[4] Hainan Meteorological Observatory and Key Laboratory of South China Sea Meterological Disaster Prevention and Mitigation of Hainan Province, Haikou, China

Submitted to *Journal of Climate*

Revised on Dec. 21, 2019

Corresponding author: Pang-Chi Hsu, Key Laboratory of Meteorological Disaster of Ministry of Education, Nanjing University of Information Science and Technology, Nanjing, China.

Email: pangchi@nuist.edu.cn; pangchi.hsu@gmail.com

Early Online Release: This preliminary version has been accepted for publication in *Journal of Climate*, may be fully cited, and has been assigned DOI 10.1175/JCLI-D-19-0337.1. The final typeset copyedited article will replace the EOR at the above DOI when it is published.

Abstract

In the summer of 2018, Northeast Asia experienced a heatwave event that broke the existing high-temperature records in several locations in Japan, the Korean Peninsula and northeastern China. At the same time, an unusually strong Madden–Julian Oscillation (MJO) was observed to stay over the western Pacific warm pool. Based on reanalysis diagnosis, numerical experiments and assessments of real-time forecast data from two subseasonal-to-seasonal (S2S) models, we discovered the importance of the western Pacific MJO in the generation of this heatwave event, as well as its predictability at the subseasonal timescale.

During the prolonged heat extreme period (11 July to 14 August), a high pressure anomaly with variability at the intraseasonal (30–90 days) timescale appeared over Northeast Asia, causing persistent adiabatic heating and clear skies in this region. As shown in the composites of MJO-related convection and circulation anomalies, the occurrence of this 30–90-day high anomaly over Northeast Asia was linked with an anomalous wave train induced by tropical heating associated with the western tropical Pacific MJO. The impact of the MJO on the heatwave was further confirmed by sensitivity experiments with a coupled GCM. As the western Pacific MJO-related components were removed by nudging prognostic variables over the tropics towards their annual cycle and longer timescales (>90 days) in the coupled GCM, the anomalous wave train along the East Asian coast disappeared and the surface air temperature in Northeast Asia reduced. The MJO over the western Pacific warm pool also influenced the predictability of the extratropical heatwave. Our assessments of two S2S models' real-time forecasts suggest that the extremity of this Northeast Asian heatwave can be better predicted 1–4 weeks in advance if the

Accepted for publication in *Journal of Climate*. DOI10.1175/JCLI-D-19-0337.1.

enhancement of MJO convections over the western Pacific warm pool is predicted well.

Key words: heat wave; Madden–Julian Oscillation; subseasonal predictability

Accepted for publication in *Journal of Climate*. DOI10.1175/JCLI-D-19-0337.1.

1. Introduction

Heatwaves, which are prolonged periods of extreme heat, have widespread impacts on human health, ecosystems, agriculture, and infrastructure. In the summer of 2018, many regions (northern Europe, North America, the Arctic Circle and Northeast Asia) experienced record-breaking high temperatures, causing immense economic damage and severe losses to human life [World Meteorological Organization (WMO) 2018]. In Northeast Asia, high temperatures above 35°C were observed in several areas in Japan, the Korean Peninsula and northeastern China. According to the Japan Meteorological Agency (JMA), the city of Kumagaya, located north of Tokyo, recorded a maximum temperature of 41.1°C on 23 July – the highest ever observed in Japan. The Korean Meteorological Administration (KMA) reported that 1 August, with a maximum temperature of 39.6°C, was the hottest day in Seoul over the past 111 years. Temperatures of up to 39°C were estimated in July and August 2018 across the northeastern provinces of China, such as Liaoning and Jilin, reported by the China Meteorological Administration (CMA). Heat-related strokes and diseases linked to the heatwave in summer 2018 caused at least 138 and 42 deaths in Japan and Korea, with more than 7,000 and 3,000 people requiring hospitalization, respectively.

Due to the severe impacts of heat extremes, understanding the mechanisms that trigger heatwave occurrence and the sources of predictability are important issues in both research and operational communities. The occurrence of heatwave events has been commonly linked to persistent high-pressure (or anticyclonic) anomalies that result in adiabatic warming via anomalous downward motion and increased solar radiation over a certain region (Della-Marta et al. 2007; Dole et al. 2011; Schubert et

Accepted for publication in *Journal of Climate*. DOI10.1175/JCLI-D-19-0337.1.

al. 2011; Lau and Kim 2012; Trenberth and Fasullo 2012; Schubert et al. 2014; Lu and Chen 2016; Gao et al. 2018). The causes of anomalous high-pressure and anticyclonic systems in different regions are various and could be related to local dynamics and remote effects. The atmospheric blocking associated with quasi-stationary Rossby waves has been found to play a primary role in heatwaves over Europe, Russia and North America (Dole et al. 2011; Schubert et al. 2011; Lau and Nath 2012; Teng et al. 2013; WMO 2018). Over East Asia, the westward extension of the western North Pacific subtropical high (WNPSH) is the key contributor to the occurrences of hot summer and heat extreme events (Li et al. 2015; Lu and Chen 2016; Gao et al. 2018; Tao and Zhang 2019). The formation of a quasi-stationary Rossby wave train and shift in the WNPSH can be further attributed to internal midlatitude dynamics and external low-boundary forcing, such as anomalous sea surface temperatures (SSTs) over different basins (Dole et al. 2011; Lau and Kim 2012; Trenberth and Fasullo 2012; Schubert et al. 2014; Lu and Chen 2016; Gao et al. 2018). For example, the European heatwave in 2010 was related to an anomalous stationary wave pattern modulated by eastern Pacific SST anomalies associated with La Niña (Dole et al. 2011; Schubert et al. 2011; Schubert et al. 2014). The anomalous quasi-stationary Rossby wave train responsible for the Russian heatwave in 2010 was correlated with SST anomalies over the tropical Atlantic and Indian oceans (Lau and Kim 2012; Trenberth and Fasullo 2012). The extension and intensification of the WNPSH, which together induce heatwaves in East China, are attributable to SST anomalies in the central-eastern equatorial Pacific (Li et al. 2015; Gao et al. 2018).

For the Northeast Asian heatwave in summer 2018, a number of recently published studies have discussed the possible contributory factors. For instance,

Accepted for publication in *Journal of Climate*. DOI10.1175/JCLI-D-19-0337.1.

Imada et al. (2019) and Qian et al. (2019) highlighted the important role of anthropogenic climate change. Specifically, based on global and regional climate model simulations, Imada et al. (2019) indicated that this record-breaking heatwave event would never have happened without anthropogenic warming. A similar conclusion was drawn by Qian et al. (2019), in which their large-ensemble simulations suggested that extreme heat events, like the Northeast Asian heatwave in 2018, are very rare without anthropogenic forcing. Not only the background warming climate but also the anomalous large-scale circulation patterns contributed significantly to the extremely hot summer in Northeast Asia in 2018 (Ha et al. 2019; Shimpo et al. 2019; Tao and Zhang 2019; Xu et al. 2019a, 2019b). In July and August 2018, the anticyclonic/subsidence anomaly that prevailed over Northeast Asia was related to the northwestward extension of the western Pacific subtropical high and the eastward expansion of the South Asian high (Ha et al. 2019; Shimpo et al. 2019; Tao and Zhang 2019; Xu et al. 2019a). This anomalous anticyclone could be further linked with the upper-tropospheric wave trains, which originate from upstream regions of 30°–100°E and propagate eastwards along the Asian westerly jet to East Asia (Tao and Zhang 2019; Xu et al. 2019b). Chen et al. (2019) suggested that the cold SST anomaly in the southeast Indian Ocean may result in anomalous cross-equatorial flow that then affects the subtropical circulations over the western North Pacific. The shift of the WNPSH led to the occurrence of the Northeast Asian heatwave in the summer of 2018.

In addition to the heating induced by tropical SST anomalies, equatorial convection associated with the Madden–Julian Oscillation (MJO; Madden and Julian 1971) can also generate large-scale circulation anomalies propagating towards extratropical regions to influence mid- and high-latitude weather regimes (Cassou

Accepted for publication in *Journal of Climate*. DOI10.1175/JCLI-D-19-0337.1.

2008; Lin et al. 2010; Moon et al. 2013; Stan et al. 2017). The MJO, characterized by planetary-scale circulation coupled with convection propagating eastwards along the equator, is the most prominent intraseasonal variability over the tropics (Madden and Julian 1971, 1972). Through altering background flows, MJO-related circulation anomalies affect weather extremes significantly in tropical areas (Yang et al. 2010; Hsu et al. 2016, 2017; Chen et al. 2018). Meanwhile, Rossby wave train patterns induced by MJO heating in the warm pool and Asian monsoon areas (Ding and Wang 2005; Moon et al. 2013) also exert impacts on weather conditions in the remote regions of North and South America, Australia and Eurasia (Jones et al. 2004; Donald et al. 2006; Lin et al. 2010; Moon et al. 2013). Such modulations of weather systems by the MJO provides a potential source of skillful prediction at lead times on the subseasonal timescale (Hsu et al. 2015; Lin 2018; Vitart and Robertson 2018), which is currently one of the most challenging tasks for operational centers (Waliser et al. 2003; Vitart et al. 2017).

As will be shown in the following analysis, abnormally intensified MJO activity over the western tropical Pacific, including the South China Sea and Philippine Sea, occurred coincidently with the Northeast Asian heatwave event in summer 2018. Were there, however, any physical links between the enhanced western tropical Pacific MJO and the occurrence of this heatwave? If yes, how and to what extent does the MJO prediction skill affect the fidelity of the extratropical heatwave forecast? These are the two key questions that will be addressed in this study. The findings could not only advance our understanding of heatwave mechanisms, but also offer a source of heatwave predictability at the subseasonal timescale – a gap between short-term weather forecasting and long-term climate prediction – that needs to be exploited in the future.

Accepted for publication in *Journal of Climate*. DOI10.1175/JCLI-D-19-0337.1.

The rest of this paper is organized as follows: The data from reanalysis and operational prediction models, the diagnostic methods, and the numerical experiments are introduced in section 2. The features and causes of the Northeast Asian heatwave in the summer of 2018 are analyzed in section 3. Section 4 verifies the essential role of the MJO in this heatwave event based on sensitivity experiments using the coupled GCM developed at the National Oceanic and Atmospheric Administration (NOAA)/Geophysical Fluid Dynamics Laboratory (GFDL). Section 5 examines the forecast skill of this heatwave in the CMA and JMA models that participated in the subseasonal-to-seasonal prediction (S2S) project (Vitart et al. 2017). A summary and some further discussion are provided in the final section.

2. Data and methods

2.1 Data

To obtain robust results, the surface air temperature (SAT) and associated circulation anomalies in the summer (June–July–August, JJA) of 2018 relative to the climatological state (1979–2017) from three global analysis/reanalysis datasets – the National Centers for Environmental Prediction (NCEP) final analysis (FNL) (NOAA/NCEP, 2000), European Centre for Medium-Range Weather Forecasts interim reanalysis (ERA-Interim) (Dee et al., 2011), and the Modern-Era Retrospective Analysis for Research and Applications, version 2 (MERRA2) (Gelaro et al. 2017) – were analyzed. In addition to the daily-mean SAT (T2m) data, three-dimensional variables including zonal and meridional wind (u and v), vertical p-velocity (ω), temperature and geopotential fields from 1000 to 100 hPa from

Accepted for publication in *Journal of Climate*. DOI10.1175/JCLI-D-19-0337.1.

ERA-Interim were also utilized. The two-dimensional fields used were surface net shortwave radiation (SSR), surface net thermal radiation (STR), sensible heat flux (SHF), and latent heat flux (LHF). The spatial resolutions of all these fields from FNL, ERA-Interim and MERRA2 were 1° × 1°, 1.5° × 1.5° and 1.5° × 1.5°, respectively. The variability and distribution of large-scale convections were illustrated by daily outgoing longwave radiation (OLR) on a 2.5° × 2.5° grid from NOAA (Liebmann and Smith, 1996).

The S2S project was established to improve our understanding of the sources of predictability and forecast skill of subseasonal-to-seasonal prediction (Vitart et al. 2017). There are 11 operational models participating in the S2S project and providing reforecasts and real-time forecasts up to 60 days. To assess the influences of equatorial MJO on predicting the Northeast Asian heatwave, we used the reforecast and real-time forecast data from two operational centers over East Asia: CMA and JMA. Note that, although KMA is also an operational center over East Asia, the variables forecasted by the KMA model are limited when it comes to comparing the prediction skill of the MJO and heatwave events against those in the CMA and JMA models. The reforecast data from the CMA and JMA models cover a common period of 1999–2010, which was used to compute the climatology of the S2S prediction. The real-time forecast frequency is daily for CMA but weekly for JMA. The CMA (JMA) model provides prediction data with a forecast time range of 60 (33) days. Four and five ensemble members are available for the CMA and JMA models, respectively. Detailed descriptions and data of these S2S models can be found on the website of the S2S dataset (https://software.ecmwf.int/wiki/display/S2S/home). The variables downloaded from the website included zonal winds at 850 and 200 hPa (U850 and U200) and OLR, used to present the MJO activity, geopotential height (H500), as

Accepted for publication in *Journal of Climate*. DOI10.1175/JCLI-D-19-0337.1.

well as SAT (T2m) for heatwave analysis.

2.2 Definitions of MJO activity

Following the method of Wheeler and Hendon (2004), we used the Real-time Multivariate MJO (RMM) index derived from the empirical orthogonal function (EOF) analysis of the combined fields of equatorially (15°S–15°N) averaged daily OLR and zonal winds at 850 and 200 hPa to define the phase evolution and intensity of the MJO. The principal components of the first two EOF modes, RMM1 and RMM2, have a quadrant phase difference and characterize the MJO signal propagating eastwards over the equatorial region. RMM1 and RMM2 can be obtained from the Australian Bureau of Meteorology (http://www.bom.gov.au/climate/mjo/graphics/rmm.74toRealtime.txt). Based on the two-dimensional phase diagram of RMM1 and RMM2, the life cycle of the MJO is split into eight distinct phases (Wheeler and Hendon 2004). In phase 1, a weak MJO convection initiates over the equatorial western Indian Ocean. It enhances and propagates eastwards towards the central and eastern Indian Ocean during phases 2–4. During the subsequent phases of 5–7, the MJO convection moves continually eastwards cross the Maritime Continent and western Pacific. It gradually dies out during phase 8 when it passes the eastern Pacific cold tongue area. The strength of the MJO is defined by the square root of the sum of squared RMM1 and squared RMM2 [$(RMM1^2+RMM2^2)^{1/2}$]. To test the effects of equatorial MJO with different strength on the extratropical conditions, two criteria for defining enhanced MJO events (RMM amplitude greater than 1 and 1.5) were used in this study.

2.3 Diagnosis of the temperature budget equation

Accepted for publication in *Journal of Climate*. DOI10.1175/JCLI-D-19-0337.1.

To understand the physical processes responsible for the SAT changes, the temperature budget equation was diagnosed. The changes in temperature at each pressure level are controlled by the horizontal temperature advection, adiabatic process associated with vertical motion and static stability, and diabatic heating, which can be written as follows:

$$\frac{\partial T'}{\partial t} = -(\mathbf{V} \cdot \nabla T)' + (\omega\sigma)' + \frac{Q'}{C_p}, \qquad (1)$$

where t is time, $\boldsymbol{V}$ is the horizontal velocity vector, ∇ is the horizontal gradient operator, and σ represents the static stability [$\sigma = \partial T / \partial p - RT / C_p P$], in which R is the gas constant, p is the pressure and C_p is the specific heat at constant pressure. The prime in Eq. (1) indicates the MJO (30–90-day) component that was obtained using the Lanczos bandpass filtering method (Duchon 1979).

As discussed by Yanai et al. (1973), the apparent heat source, Q, includes the radiative heating, latent heat release, and surface turbulent heat fluxes. At the planetary boundary layer, Q is largely modulated by the net upward flux through the surface (Fs). To understand the major contributors to the near-surface heat source, the surface energy budget equation, shown in Eq. (2), was further diagnosed:

$$\text{Fs}=\text{SSR}+\text{STR}+\text{SHF}+\text{LHF}+\text{G}. \qquad (2)$$

Here, SSR and STR are the net shortwave and thermal (longwave) radiation at the surface, respectively; SHF and LHF denote the sensible and latent heat fluxes, respectively; and G, the ground heat flux, is generally small and can be ignored in this study. All fluxes are positive upward.

Accepted for publication in *Journal of Climate*. DOI10.1175/JCLI-D-19-0337.1.

2.4 Model experiments

To understand the influences of tropical heating at the subseasonal timescale on the SAT and circulation changes over northeastern Asia, we performed model experiments using the GFDL Low Ocean Atmosphere Resolution (LOAR; van der Wiel et al. 2016) of Coupled Model 2.5 (CM2.5; Delworth et al. 2012), which has high capability in simulating the MJO (Xiang et al. 2015). The atmospheric/land-surface components of the LOAR model have a C48 grid horizontal resolution (2° × 2°) with 32 vertical levels. The ocean/sea ice components have 1° × 1° horizontal grids.

With a focus on natural variability, the control experiment (EXP_CTRL) was integrated for 70 years with the constant radiative forcing in 1990. Using the same radiative forcing, the sensitivity experiment was also integrated for 70 years but the model prognostic variables (e.g., u, v, q, T) over tropical regions (15°S–15°N) were nudged towards their 90-day low-pass (LP90) filtered components derived from the control experiment. In this case, the equatorial subseasonal variability with a periodicity shorter than 90 days was removed artificially, while other tropical variations with periodicities of longer than 90 days were retained in the model. The sensitivity experiment is referred to as EXP_LP90. Comparing the large-scale circulation and SAT over Northeast Asia simulated from EXP_CTRL and EXP_LP90, one may verify the effects of tropical subseasonal heating on the extratropical atmospheric conditions.

3. Features of the northeastern Asian heatwave in 2018 and the effects of the

Accepted for publication in *Journal of Climate*. DOI10.1175/JCLI-D-19-0337.1.

MJO

Compared to the climatological summer (JJA)-mean SAT, remarkable increases in SAT occurred over Eurasia in the summer of 2018 according to all the datasets (Figs. 1a–c). ERA-Interim and MERRA2 consistently reveal that the maximum of positive SAT anomalies in the summer of 2018 appeared over Northeast Asia, including northeastern China, the Korean Peninsula and Japan (rectangles in Figs. 1a and 1b). Although less evident, the positive SAT anomaly over Northeast Asia is also apparent in the FNL data (Fig. 1c). The area-averaged SAT over Northeast Asia (32.5°−47.5°N, 110°−140°E) reached 23°C−27°C (around 3°C higher than the climatology) from mid-July to mid-August (Figs. 1d–f), when the record-breaking heatwave events in northeastern China, Korea and Japan were reported (marked by gray shading in Figs. 1d–f). Two peaks of SAT anomalies around 21 July and 1 August both exceed the values of the 90th percentile (green dots in Figs. 1d–f).

The Northeast Asian extreme heat in the summer of 2018 occurred consistently with high-pressure anomalies associated with the eastward expansion of the South Asian high (Fig. 2a) and the northwestward extension of the WPSH (Fig. 2b), consistent with previous results (Shimpo et al. 2019; Tao and Zhang 2019; Xu et al. 2019a, 2019b). To further discuss the temporal evolution of the high anomalies within the summer season, we examined the area-averaged 200- and 500-hPa geopotential height anomalies, in which the seasonal cycle was removed, over the heatwave occurrence region (Figs. 2c, d). The daily geopotential height anomalies varied at the intraseasonal timescale with a period of ~30–90 days (red curves in Figs. 2b and 2d). The positive anomalies of geopotential height increased significantly from mid-July to early August, consistent with the timing of heatwave occurrence and maintenance.

Accepted for publication in *Journal of Climate*. DOI10.1175/JCLI-D-19-0337.1.

The low-frequency circulation anomaly situated over Northeast Asia provided favorable conditions for the occurrence of a prolonged heatwave. Figure 3a displays the phase relationship between 30–90-day height and SAT anomalies. During the heatwave period, the 30–90-day high-pressure anomaly is highly consistent with the increased SAT anomaly over Northeast Asia. The positive anomaly of 30–90-day SAT over Northeast Asia is around 0.5°C–1.5°C (Fig. 3a), accounting for 20%–60% of the total increases in SAT (2.5°C–3°C) associated with this heatwave event (Figs. 1d–f). Based on diagnosis of the temperature budget, the major contributor to the increases in SAT anomalies was the adiabatic heating (Fig. 3b) caused by anomalous descending motion associated with the high-pressure anomaly. The circulation anomalies also led to positive warm advection, favoring the heatwave's occurrence (Fig. 3b).

To further elucidate the source of negative diabatic heating anomaly near the surface, we diagnosed the surface energy budget using the same ERA-Interim reanalysis dataset (Fig. 3c). The results show that the high anomaly-induced subsidence and clear sky favored increased downward shortwave radiation (SSR in Fig. 3c), which heated the surface. The increased surface heat was further radiated back to the atmosphere as an upward thermal radiation (STR) anomaly and returned to the atmosphere by enhanced SHF. The LHF associated with precipitation and evapotranspiration also contributed positively to heat the atmosphere during the heatwave period. Their net effect (a downward heat flux) would have led to a warmer surface temperature than the SAT. Although the surface energy budget result seems to be consistent with the 925-hPa air temperature budget, the estimations for each budget term still contain some uncertainty because of precipitation, cloud and

Accepted for publication in *Journal of Climate*. DOI10.1175/JCLI-D-19-0337.1.

radiation biases in the reanalysis system (Ma et al. 2018).

Based on the results of Figs. 1–3, the high-pressure anomaly, which seems to be part of the low-frequency (30–90-day) wave train, played a key role in the record-breaking heatwave over Northeast Asia in the summer of 2018. To understand the source of the 30–90-day large-scale circulation anomalies, we examined the tropical heating distributions, as previous studies (Nitta 1987; Lu 2001; Kosaka and Nakamura 2006; Hsu and Lin 2007) have suggested that the anomalous convection over the western Pacific warm pool region associated with seasonal SST anomalies can generate a Rossby wave train and propagate towards the midlatitudes. At the intraseasonal timescale, convection over the warm pool is closely modulated by the MJO (Madden and Julian 1971, 1994). Figure 4 shows the phase evolutions of the MJO in summer 2018. Interestingly, the equatorial MJO convection stayed persistently in the RMM phases 5–6 with abnormally strong intensity (RMM amplitude of 1.5–2) during the heatwave period of 11 July to 14 August (Fig. 4a). This distribution of 30–90-day OLR clearly shows the presence of enhanced convection over the western Pacific warm pool, including the South China Sea and Philippine Sea, during this heatwave event (Fig. 4b). The results suggest that the enhanced MJO convective heating could have induced the anomalous wave train pattern associated with the extratropical heatwave occurrence.

To further elucidate the basic structures and dynamics of the wave train pattern, we examined the 30–90-day vorticity and the wave activity flux (WAF), defined by Takaya and Nakamura (2001), at different levels. As shown in Fig. 5, 30–90-day wavelike structures with a zonally elongated cyclonic anomaly over the South China Sea and Philippine Sea and an anticyclonic anomaly over the Northeast Asia appeared

Accepted for publication in *Journal of Climate*. DOI10.1175/JCLI-D-19-0337.1.

during the heatwave period (Figs. 5a–c). These anomalous wavelike patterns along the western Pacific–East Asian coast present an equivalent barotropic vertical structure titling slightly polewards with height. The lower- and mid-tropospheric WAF exhibits northward-pointing vectors from the tropical western Pacific towards Northeast Asia (~40°N), suggesting a Rossby wave–like energy propagation (Figs. 5a–b). In contrast, in the upper troposphere, eastward WAF at 40°–50°N is evident, and southward WAF over East Asia is also apparent (Fig. 5b). The vertical structures and WAF of the intraseasonal wave train here (Fig. 5) resemble the Pacific–Japan pattern at the long-term (i.e., monthly, seasonal and interannual) timescales identified by previous studies (Nitta 1987; Kosaka and Nakamura 2006; Hsu and Lin 2007).

The large-scale circulation anomalies over extratropical regions vary with MJO-related heating of different amplitude and are situated in different locations (Ding and Wang 2007; Moon et al. 2013; Stan et al. 2017). As the western Pacific MJO convection started to establish (phases 3–4) and strengthen (phases 5–6), significant high-pressure anomalies appeared and prevailed over Eurasia at the mid and high latitudes (Figs. 6b and 6c). The extratropical circulation anomalies were enhanced as the MJO convections became stronger (Figs. 6f and 6g). Once suppressed MJO convections appeared over the western Pacific warm pool regions (phases 7–8 and 1–2), the midlatitude high-pressure anomalies moved polewards (Figs. 6a, d, e, h), but a low-pressure anomaly occurred over East/Northeast Asia (Figs. 6d and 6h). Circulation and SAT anomalies induced by western Pacific MJO heating can sustain for around two weeks. Consistent with the result of Fig. 6, the positive anomalies of geopotential height and SAT over Northeast Asia were of stronger amplitude as the equatorial heating of the MJO intensified (Fig. 7). The increased SAT, with its amplitude greater than 0.8 standard deviations, was able to

Accepted for publication in *Journal of Climate*. DOI10.1175/JCLI-D-19-0337.1.

last 11 (9) days when the MJO's amplitude was greater than 1.5 (1), as equatorial heating tends to induce a relatively stronger (weaker) high-pressure anomaly over Northeast Asia.

The analyses above suggest a positive contribution of the western tropical Pacific MJO to the Northeast Asian heatwave in the summer of 2018. Whether or not the MJO's effect on this heatwave in 2018 is a unique case is worthy of discussion. To address this, we analyzed the phase relationship between the MJO's evolution and Northeast Asian heatwave events using long-term historical data from 40 summers (1979–2018). A long-lasting heatwave over Northeast Asia was defined when the area-averaged (32.5°–47.5°N, 110°–140°E) SAT was higher than the 75th percentile for 10 consecutive days or more. The individual days during each heatwave event are referred to as heatwave days. Taking the annual cycle of SAT into account, the thresholds of SAT (i.e., the 75th percentile) for each day (t) were derived from SAT data during the period between t − 7 (7 days before t) and t + 7 (7 days after t) for the period 1979–2018, with total samples of 600 (15 days × 40 years), similar to the method proposed by Stefanon et al. (2012). Figure 8 displays the states of the MJO's life cycle for individual heatwave days from the climatological viewpoint. It is apparent that around 50% of Northeast Asian heatwaves in history occurred when the MJO's convection was enhanced over the western Pacific warm pool (phases 5–6). The increases in heatwave occurrence rate in phases 5–6 are statistically significant based on the Monte Carlo test. Much smaller probabilities (0.8%–14%) of Northeast Asian heatwave occurrence are found when the MJO stays over the tropical Indian Ocean and central-eastern Pacific (Fig. 8a). The average probability (25%) of heatwave occurrence in phasees 5–6 is about three times larger than that in the other

Accepted for publication in *Journal of Climate*. DOI10.1175/JCLI-D-19-0337.1.

six phases (8%). Considering the persistence of MJO-induced anomalous states (Fig. 7), we included the data from 7 days before heatwave occurrence and repeated the analysis. The results showed that more than half (51.1%) of the prolonged heat extremes occurred in phases 5–6 of the MJO (Fig. 8b), suggesting that the western Pacific MJO does indeed play a role in the generation and maintenance of Northeast Asian heatwaves. Note that the results are robust and did not change even when the criteria for the definition of a heatwave were varied. For example, ~50% of Northeast Asian heatwave days appeared in conjunction with MJO phases 5–6 when a regional heatwave event was defined by the daily SAT exceeding the 95th percentile for at least three consecutive days (not shown).

Additional analysis by calculating the SAT anomalies during summers with vigorous western Pacific MJO activities was conducted to confirm the effect of the MJO on the occurrence of Northeast Asian hot summers. To quantify the effect of the western Pacific MJO, the accumulated amplitude of phases 5–6 occurring during July to August was defined and referred to as the western Pacific MJO index. This index combines the effects of frequency and intensity of western Pacific MJO events (phases 5–6) in each summer. Then, the years with a normalized western Pacific MJO index greater than 1.5 standard deviations were selected for SAT composites and compared against the climatological state. The results showed that the Northeast Asian SAT increased significantly in summers with vigorous western Pacific MJO activities (figures not shown), confirming the positive contribution of western Pacific MJO convections to Northeast Asian heat events.

4. Sensitivity experiments for verifying the role of the MJO in the heatwave

Accepted for publication in *Journal of Climate*. DOI10.1175/JCLI-D-19-0337.1.

Using reanalysis diagnosis, it is difficult to isolate the effects of the MJO heating on the large-scale anticyclonic anomalies (Figs. 5–6) that induced the heatwave over Northeast Asia. To verify whether the anomalous circulations in the extratropics were related to the abnormally persistent and enhanced MJO states in phases 5–6, we conducted a model experiment using the LOAR coupled GCM, which simulates MJO signals well over the equatorial area (Xiang et al. 2015). The composites of MJO-related convections based on the days with enhanced MJO convection occurring over the tropical western Pacific (0°−15°N, 100°−150°E), mimicking the RMM phases 5−6, are shown in Figs. 9a and 9b. The active western Pacific MJO days were selected as when the area-averaged 30−90-day OLR over the western Pacific exceeded 1 and 1.5 standard deviations, respectively. Thus, significant MJO convections over the western tropical Pacific were detected in the composite map in EXP_CTRL (Fig. 9a). The strategy of MJO removal by nudging the prognostic fields towards their climatological annual cycle derived from EXP_CTRL worked efficiently. Using the same days with western Pacific convections in EXP_CTRL, the composite map showed no MJO signals over the equatorial region (Figs. 9b and 9e). This means that the effect of tropical western Pacific MJO heating was absent in EXP_LP90. Comparing the SAT anomalies over Northeast Asia (32.5°−47.5°N, 110°−140°E), the positive SAT anomaly in EXP_CTRL dropped when the western Pacific MJO was removed (Figs. 9c and 9f).

The change in SAT could be attributable to the anomalous wave train induced by the western Pacific MJO convection. Similar to the observation, the high anomaly appeared over Northeast Asia when the western Pacific MJO heating generated an anomalous wave train along the East Asian coast in EXP_CTRL (Fig. 10a). In

Accepted for publication in *Journal of Climate*. DOI10.1175/JCLI-D-19-0337.1.

contrast, this south–north-oriented wave train and the related high anomaly over Northeast Asia vanished in EXP_LP90 as the tropical MJO components were removed (Fig. 10b). Thus, the SAT tended to reduce in EXP_LP90 (Fig. 9c). The decrease in the SAT anomaly over the Northeast Asian heatwave region was more obvious if the more strengthened MJO convections over the tropical western Pacific (with amplitude greater than 1.5 standard deviations) were removed from the model integration (Figs. 9d–f). The results of these sensitivity experiments using the coupled GCM confirm the role of intraseasonal heating over the tropical western Pacific in causing the SAT anomalies in Northeast Asia.

5. Subseasonal prediction of the heatwave

Profound influences of enhanced MJO over the western Pacific on this Northeast Asian heatwave event have thus far been found based on observational and sensitivity experiment results. However, whether or not the equatorial MJO can serve as a key source of predictability for extratropical heatwaves at the subseasonal range also needs to be assessed. Using the reforecasts and real-time forecasts of the CMA and JMA S2S models, we next assess the forecast skill of the present heatwave case at the subseasonal timescale and discuss how it was affected by the prediction of the equatorial MJO.

The capability of SAT predictions during the observed heatwave period (11 July to 14 August) was analyzed based on real-time forecasts with lead times of 1 to 4 weeks (Fig. 11). The one-week-lead forecast skill for the period covering the weeks of 11–17 July, 18–24 July, 25–31 July, 1–7 August, and 8–14 August was assessed

Accepted for publication in *Journal of Climate*. DOI10.1175/JCLI-D-19-0337.1.

using the predicted results of 0–6 days from the forecasts started at 11 July, 18 July, 25 July, 1 August, and 8 August, respectively. Likewise, the two-week-lead forecast skill for the same period covering the weeks of 11–17 July, 18–24 July, 25–31 July, 1–7 August, and 8–14 August was evaluated using the predicted results of 7–13 days from the forecasts started at 4 July, 11 July, 18 July, 25 July, and 1 August, respectively. A similar approach was applied to the skill assessments for the three- and four-week-lead forecasts. The SAT anomalies were computed relative to the model climatology derived from the reforecasts of 1999–2010.

At the lead time of 1 week (blue curve), the CMA and JMA models both captured the temporal evolutions of the SAT anomalies with an increasing tendency from the first week (11–17 July) and a decreasing tendency from the third week (25 July to 14 August). The two models, however, revealed significant biases in the amplitude of SAT anomalies. In the CMA model, the SAT anomalies were overestimated (Fig. 11a), while in the JMA model small positive anomalies of SAT were predicted (Fig. 11b). Some members even predicted negative SAT anomalies over the Northeast Asian heatwave region in the JMA model (Fig. 11b).

The predicted biases of SAT associated with this heatwave event were likely linked with the biased amplitude of MJO predictions and the MJO-related circulation anomalies in the two operational models. We compared the predicted MJO index, large-scale circulation anomaly and SAT in the fixed period of 11 July to 14 August produced by the forecasts with different initial dates. For example, the predicted results for 11 July to 14 August produced by the forecast started on 4 July (27 June) were considered to be a forecast at a lead time of 7–40 (14–54) days (Fig. 12). Although the CMA model correctly predicted the locations of MJO convection

Accepted for publication in *Journal of Climate*. DOI10.1175/JCLI-D-19-0337.1.

(phases 5–6) in the long forecast leads beyond three weeks (blue, red and green curves in Fig. 12a), the amplitude of MJO convections appeared to be too high compared to the observation. This might have caused the overestimated SAT anomalies in Northeast Asia (Fig. 11a), because the SAT and high-pressure anomalies over the midlatitudes were positively correlated with the strength of tropical heating (Figs. 12b and c). Similarly, the weak MJO convections predicted by the JMA model (Fig. 12d) could only result in a weak response of atmospheric conditions over the extratropics (Fig. 12f), and led to insignificant changes in SAT in the Northeast Asian heatwave area (Fig. 12e). The results based on the assessments of the S2S models suggest that the subseasonal predictability of Northeast Asian heatwaves is to a certain extent affected by the fidelity of MJO prediction.

6. Summary and discussion

During 11 July to 14 August 2018, a record-breaking heatwave with temperatures of ~3°C higher than the climatology (exceeding the 90th percentile) affected large portions of Northeast Asia, including Japan, the Korean Peninsula and northeastern China (WMO 2018) (Fig. 1). Some recent works (Chen et al. 2019; Ha et al. 2019; Imada et al. 2019; Shimpo et al. 2019; Tao and Zhang 2019) have emphasized the contributions of anthropogenic climate change and seasonal circulation anomalies to this Northeast Asian heatwave event. In addition to the anomalous summer-mean conditions, we found that the subseasonal signals associated with the western Pacific warm pool MJO (phases 5–6 of the RMM) also revealed abnormality in its duration and amplitude during the heatwave event period. Based on reanalysis diagnosis and model experiments, we have further proven the

Accepted for publication in *Journal of Climate*. DOI10.1175/JCLI-D-19-0337.1.

important role played by the western tropical Pacific MJO in the generation and maintenance of this Northeast Asian heatwave event. The effect of the MJO on the heatwave prediction skill at the subseasonal timescale has also been revealed, by assessing the S2S models of two operational centers in East Asia (the CMA and JMA).

The prolonged heat conditions can be attributed to the occurrence of a persistent high-pressure anomaly with a pronounced feature of low-frequency (30–90 days) variability over Northeast Asia (Fig. 2), which caused anomalous downward motion favoring clear skies and adiabatic heating locally (Fig. 3). The occurrence and maintenance of such a high-pressure anomaly over Northeast Asia are further related to enhanced MJO convection over the western Pacific warm pool via atmospheric teleconnection (Cassou 2008; Lin et al. 2010; Moon et al. 2013; Stan et al. 2017). In the MJO phase diagram (Fig. 4), abnormally intensified MJO activities (staying at phases 5–6) were observed consistently during the heatwave period. The persistence of MJO-related heating in the western tropical Pacific may have excited a Rossby wave train (Fig. 5) with a low-pressure anomaly to the north of the MJO convection and a high-pressure anomaly over Eurasia, including Northeast Asia (Fig. 6). The high-pressure anomaly may have persisted around two weeks after the occurrence of tropical MJO heating (Fig. 7), providing a favorable environment for prolonged high SATs over Northeast Asia. During the summers of 1979–2018, around 50% of Northeast Asian heatwave days occurred at and after the RMM phases 5–6. The probability of heatwave occurrence in phases 5–6 is about three times higher than that in other phases (Fig. 8). These statistical analyses reveal the contribution of western tropical Pacific MJO to the formation and maintenance of Northeast Asian heatwaves.

Accepted for publication in *Journal of Climate*. DOI10.1175/JCLI-D-19-0337.1.

Based on sensitivity experiments with the GFDL LOAR coupled GCM, which simulates tropical MJO signals well, we again confirmed the contribution of the western tropical Pacific MJO to this Northeast Asian heatwave. When the subseasonal components over the tropics (15°S–15°N) were removed by nudging the prognostic fields towards their annual cycle and longer timescales (>90 days) derived from EXP_CTRL, the anomalous wave train along the East Asian coast vanished and the SAT over the Northeast Asian heatwave area was reduced compared to that in EXP_CTRL, in which the enhanced western Pacific MJO remained (Figs. 9 and 10).

The importance of MJO-related heating over the western Pacific warm pool was also seen from the viewpoint of heatwave prediction at the subseasonal timescale. Through assessing the real-time forecast data of the CMA and JMA S2S models, we found that the predicted MJO conditions were linked closely with the forecast capability for this Northeast Asian heatwave event. The CMA model predicted the location of enhanced MJO convection well over the western tropical Pacific (phases 5–6) during the heatwave period at forecast leads beyond three weeks. However, it overestimated the MJO amplitude (Fig. 12a). The high SAT anomalies over the Northeast Asian heatwave region were predicted with overestimated biases by the CMA model (Fig. 11a). In contrast, the Northeast Asian SAT showed insignificant changes when the weak MJO signals were predicted by the JMA model at the subseasonal timescale (Figs. 11b and 12d). Thus, the subseasonal prediction skill for heat extremes over Northeast Asia seems to benefit from more accurate predictions of the MJO in S2S models. The result suggests that the MJO plays a key role in the subseasonal predictability of extratropical heat extreme, as documented by Lin (2018) and Vitart and Roberson (2018).

Accepted for publication in *Journal of Climate*. DOI10.1175/JCLI-D-19-0337.1.

Predicting extreme events more than two weeks in advance remains a challenging task. In this study, we emphasize the effects of the MJO on heatwave predictability at the subseasonal timescale. Recent works have found that air–sea interaction (Lin 2018), land conditions (Orth and Seneviratne 2014; National Academies of Sciences, Engineering and Medicine, 2016), and stratosphere–troposphere coupling (Mundhenk et al. 2018) might also serve as potential sources of subseasonal predictability. How and to what extent these factors contribute to the subseasonal prediction of heatwaves and other extreme events in the densely populated Asian monsoon region needs to be further investigated.

Acknowledgements

The authors would like to thank the anonymous reviewers for their comments, which helped to improve the manuscript. This work was supported by the National Key Research and Development Program of China (2018YFC1505804).

Accepted for publication in *Journal of Climate*. DOI10.1175/JCLI-D-19-0337.1.

References:

Cassou, C., 2008: Intraseasonal interaction between the Madden-Julian Oscillation and the North Atlantic Oscillation. *Nature*, **455**, 523–527.

Chen R., Z. Wen, and R. Lu, 2018: Large-scale circulation anomalies and intraseasonal oscillations associated with long-lived extreme heat events in South China. *J. Climate*, 31, 213–232.

Chen R., Z. Wen, and R. Lu, 2019: Influences of tropical circulation and sea surface temperature anomalies on extreme heat over Northeast Asia in the midsummer of 2018. *Atmospheric and Oceanic Science Letters,* **12**, 238–245. doi: 10.1080/16742834.2019.1611170.

Dee D. P., and Coauthors, 2011: The ERA-Interim reanalysis: configuration and performance of the data assimilation system. *Quart J. Roy. Meteorol. Soc.*, **137**, 553–597.

Della-Marta, P., J. Luterbacher, H. von Weissenfluh, E. Xoplaki, M. Brunet, and H. Wanner, 2007: Summer heat waves over western Europe 1880–2003, their relationship to large-scale forcings and predictability. *Clim. Dyn.*, **29**, 251–275.

Delworth, T. L., and Coauthors, 2012: Simulated climate and climate change in the GFDL CM2.5 high-resolution coupled climate model. *J. Climate*, **25**, 2755–2781.

Ding, Q., and B. Wang, 2007: Intraseasonal teleconnection between the summer Eurasian wave train and the Indian monsoon. *J. Climate*, **20**, 3751–3767.

Dole, R., and Coauthors, 2011: Was there a basis for anticipating the 2010 Russian

Accepted for publication in *Journal of Climate*. DOI10.1175/JCLI-D-19-0337.1.

heat wave? *Geophys. Res. Lett.*, **38**, L06702.

Donald, A., H. Meinke, B. Power, A. H. N. Maia, M. C. Wheeler, N. White, R. C. Stone, and J. Ribbe, 2006: Near-global impact of the Madden-Julian oscillation on rainfall. *Geophys. Res. Lett.*, **33**, L09704.

Duchon, C. E., 1979: Lanczos filtering in one and two dimensions. *J. Appl. Meteor.*, **18**, 1016–1022.

Gao, M., B. Wang, J. Yang, and W. Dong, 2018: Are peak summer sultry heat wave days over the Yangtze-Huaihe River basin predictable? *J. Climate*, **31**, 2185–2196.

Gelaro, R., and Coauthors, 2017: The Modern-Era Retrospective Analysis for Research and Applications, Version 2 (MERRA-2). *J. Climate*, **30**, 5419–5454.

Ha, K-J, J-H Yeo, Y-W Seo, E-S Chung, J-Y Moon, X. Feng, Y-W Lee and C-H Ho, 2019: What caused the extraordinarily hot 2018 summer in Korea? *J. Meteorol. Soc. Japan*, published online, DOI: 10.2151/jmsj.2020-009.

Hsu, H.-H., and S.-M. Lin, 2007: Asymmetry of the tripole rainfall pattern during the East Asian summer. *J. Climate*, **20**, 4443–4458.

Hsu P.-C., T. Li, L. You, J. Gao, and H.-L. Ren, 2015: A spatial-temporal projection model for 10-30 day rainfall forecast in South China. *Clim. Dyn.*, **44**, 1227–1244.

Hsu, P.-C., J.-Y. Lee, and K.-J. Ha, 2016: Influence of boreal summer intraseasonal oscillation on rainfall extremes in southern China. *Int. J. Climatol.*, **36**, 1403–1412.

Hsu, P.-C., J.-Y. Lee, K.-J. Ha, and C.-H. Tsou, 2017: Influences of boreal summer intraseasonal oscillation on heat waves in monsoon Asia. *J. Climate*. **30**, 7191–

Accepted for publication in *Journal of Climate*. DOI10.1175/JCLI-D-19-0337.1.

7211.

Imada, Y., M. Watanabe, H. Kawase, H. Shiogama, and M. Arai, 2019: The July 2018 high temperature event in Japan could not have happened without human-induced global warming. *SOLA*, **15A**, 8−12, doi:10.2151/sola.15A-002.

Jones, C., D. E. Waliser, K. Lau, and W. Stern, 2004: Global occurrences of extreme precipitation and the Madden-Julian Oscillation: Observations and predictability. *J. Climate*, **17**, 4575–4589.

Kosaka, Y., and H. Nakamura, 2006: Structure and dynamics of the summertime Pacific-Japan (PJ) teleconnection pattern. *Quart. J. Roy. Meteor. Soc.*, **132**, 2009–2030.

Lau, N.-C., and M. J. Nath, 2012: A model study of heat waves over North America: Meteorological aspects and projections for the twenty-first century. *J. Climate*, **25**, 4761–4784.

Lau, W. K. M., and K.-M. Kim, 2012: The 2010 Pakistan flood and Russian heat wave: Teleconnection of hydrometeoro- logical extremes. *J. Hydrometeor.*, **13**, 392–403.

Li, J., T. Ding, X. Jia, and X. Zhao, 2015: Analysis on the extreme heat wave over China around Yangtze River region in the summer of 2013 and its main contributing factors. *Adv. Meteor.*, 706713.

Liebmann B., and C. A. Smith, 1996: Description of a complete (interpolated) outgoing long wave radiation dataset. *Bull. Amer. Meteor. Soc.*, **77**, 1275–1277.

Lin, H., G. Brunet, and R. Mo, 2010: Impact of the Madden-Julian Oscillation on

Accepted for publication in *Journal of Climate*. DOI10.1175/JCLI-D-19-0337.1.

wintertime precipitation in Canada. *Mon. Wea. Rev.*, **138**, 3822–3839.

Lin, H., 2018: Predicting the dominant patterns of subseasonal variability of wintertime surface air temperature in extratropical Northern Hemisphere. *Geophys. Res. Letts*., **45**, 4381–4389.

Lu, R. Y., 2001: Interannual variability of the summertime North Pacific subtropical high and its relation to atmospheric convection over the warm pool. *J. Meteor. Soc. Japan Ser. II*, **79**, 771–783.

Lu, R., and R. Chen, 2016: A review of recent studies on extreme heat in China, *Atmospheric and Oceanic Science Letters*, **9**, 114–121.

Ma H.-Y., S. A. Klein, S. Xie, C. Zhang, S. Tang, Q. Tang, C. J. Morcrette, K. Van Weverberg, J. Petch, M. Ahlgrimm, L. K. Berg, F. Cheruy, J. Cole, R. Forbes, W. I. Gustafson Jr, M. Huang, Y. Liu, W. Merryfield, Y. Qian, R. Roehrig, and Y.-C. Wang, 2018: CAUSES: On the role of surface energy budget errors to the warm surface air temperature error over the Central United States. *J. Geophys. Res.*, **123**, 2888– 2909. https://doi.org/10.1002/2017JD027194.

Madden R. A., and P. R. Julian, 1971: Detection of a 40-50 day oscillation in the zonal wind in the tropical Pacific. *J. Atmos. Sci.*, **28**, 702–708.

Madden R. A., and P. R. Julian, 1972: Description of global-scale circulation cells in the tropics with a 40-50 day period. *J. Atmos. Sci.*, **29**, 1109–1123.

Madden R. A., and P. R. Julian, 1994: Observations of the 40-50 day tropical oscillation—A review. *Mon. Wea. Rev.*, **122**, 814–837.

Moon J.-Y., Wang B, Ha K.-J., and Lee J.-Y.. 2013: Teleconnections associated with

Accepted for publication in *Journal of Climate*. DOI10.1175/JCLI-D-19-0337.1.

Northern Hemisphere summer monsoon intraseasonal oscillation. *Clim. Dyn.*, **40**, 2761–2774.

Mundhenk B. D., E. A. Barnes, E. D. Maloney, and C. F. Baggett, 2018: Skillful empirical subseasonal prediction of landfalling atmospheric river activity using the Madden–Julian oscillation and quasi-biennial oscillation. *npj Climate and Atmospheric Science*, **1**, 20177.

National Academies of Sciences, Engineering and Medicine, 2016: *Next generation Earth system prediction (2016), strategies for subseasonal to seasonal forecasts*. Washington, DC: The National Academies Press. https://doi.org/10.17226/2187

Nitta, T., 1987: Convective activities in the tropical western Pacific and their impact on the northern hemisphere summer circulation. *J. Meteor. Soc. Japan*, **65**, 373–390.

NOAA/NCEP, 2000: NCEP FNL Operational Model Global Tropospheric Analyses, continuing from July 1999 (updated daily). NCAR Computational and Information Systems Laboratory Research Data Archive, accessed 30 August 2018, https://doi.org/10.5065/D6M043C6.

Orth, R., and S. I. Seneviratne, 2014: Using soil moisture forecasts for sub-seasonal summer temperature predictions in Europe. *Clim. Dyn.*, 43, 3403-3418.

Qian Y., H. Murakami, P-C Hsu, and S. B. Kapnick, 2019: Effects of anthropogenic forcing and natural variability on the 2018 heatwave in Northeast Asia, *Bull. Amer. Meteor. Soc.*, published online, DOI:10.1175/BAMS-D-19-0156.1.

Schubert, S., H. Wang, and M. Suarez, 2011: Warm season subseasonal variability

Accepted for publication in *Journal of Climate*. DOI10.1175/JCLI-D-19-0337.1.

and climate extremes in the Northern Hemisphere: The role of stationary Rossby waves. *J. Climate*, **24**, 4773–4792.

Schubert, S., H. Wang, D. Randal, and M. Suarez, 2014: Northern Eurasian Heat Waves and Droughts. *J. Climate*, **27**, 3169–3207.

Shimpo, A., K. Takemura, S. Wakamatsu, H. Togawa, Y. Mochizuki, M. Takekawa, S. Tanaka, K. Yamashita, S. Maeda, R. Kurora, H. Murai, N. Kitabatake, H. Tsuguti, H. Mukougawa, T. Iwasaki, R. Kawamura, M. Kimoto, I. Takayabu, Y. Takayabu, Y. Tanimoto, T. Hirooka, Y. Masumoto, M. Watanabe, K. Tsuboki, and H. Nakamura, 2019: Primary factors behind the Heavy Rain Event of July 2018 and the subsequent heat wave in Japan. *SOLA*, **15A**, 13−18, doi:10.2151/sola.15A-003.

Stan, C., D. M. Straus, J. S. Frederiksen, H. Lin, E. D. Maloney, and C. Schumacher, 2017: Review of tropical-extratropical teleconnections on intraseasonal time scales. *Rev. Geophys.*, **55**, 902–937.

Stefanon, M., F. D’Andrea, and P. Drobinski, 2012: Heatwave classification over Europe and the Mediterranean region. *Environ. Res. Lett.*, **7**, 014023.

Takaya, K., and H. Nakamura, 2001: A formulation of a phase-independent wave-activity flux for stationary and migratory quasigeostrophic eddies on a zonally varying basic flow. *J. Atmos. Sci.*, **58**, 608–627.

Tao, P., and Y. Zhang, 2019: Large-scale circulation features associated with the heat wave over Northeast China in summer 2018, *Atmospheric and Oceanic Science Letters*, in press, doi: 10.1080/16742834.2019.1610326.

Accepted for publication in *Journal of Climate*. DOI10.1175/JCLI-D-19-0337.1.

Teng, H., G. Branstator, H. Wang, G. A. Meehl, and W. M. Washington, 2013: Probability of US heat waves affected by a subseasonal planetary wave pattern. *Nature Geosci.*, **6**,1056–1061.

Trenberth, K. E., and J. T. Fasullo, 2012: Climate extremes and climate change: The Russian heat wave and other climate extremes of 2010. *J. Geophys. Res.*, **117**, D17103.

van der Wiel, K., and Coauthors, 2016: The resolution dependence of contiguous U.S. precipitation extremes in response to CO2 forcing. *J. Climate,* **29,** 7991–8012.

Vitart, F., and coauthors, 2017: The subseasonal to seasonal prediction (S2S) project database. *Bull. Amer. Meteor. Soc.*, **98**, 163–173.

Vitart, F., and W. A. Robertson, 2018: The sub-seasonal to seasonal prediction project (S2S) and the prediction of extreme events. *npj Climate and Atmospheric Science*, **1**, 3.

Waliser, D. E., K.-M. Lau, W. Stern, and C. Jones, 2003: Potential predictability of the Madden-Julian Oscillation. *Bull. Amer. Meteor. Soc.*, **84**, 33–50.

Wheeler M. C., and H. H. Hendon, 2004: An all-season real-time multivariate MJO index: development of an index for monitoring and prediction. *Mon. Wea. Rev.*, **132**, 1917–1932.

World Meteorological Organization (WMO), 2018: “July sees extreme weather with high impacts”, Retrieved 1 August 2018 at the website of https://public.wmo.int/en/media/news/july-sees-extreme-weather-high-impacts.

Xiang, B., M. Zhao, X. Jiang, S.-J. Lin, T. Li, X. Fu, and G. Vecchi, 2015: 3–4 week

Accepted for publication in *Journal of Climate*. DOI10.1175/JCLI-D-19-0337.1.

MJO prediction skill in a GFDL Coupled Model. *J. Climate*, **28**, 5351–5364.

Xu K., R. Lu, J. Mao, and R. Chen, 2019a: Circulation anomalies in the mid–high latitudes responsible for the extremely hot summer of 2018 over northeast Asia, *Atmospheric and Oceanic Science Letters*, **12**, 231–237, DOI: 10.1080/16742834.2019.1617626

Xu, K., R. Lu, B.-J. Kim, J.-K. Park, J. Mao, J.-Y. Byon, R. Chen, and E.-B. Kim, 2019b: Large-Scale Circulation Anomalies Associated with Extreme Heat in South Korea and Southern–Central Japan. *J. Climate*, **32**, 2747–2759.

Yanai, M., S. Esbensen, and J.-H. Chu, 1973: Determination of bulk properties of tropical cloud clusters from large-scale heat and moisture budgets. *J. Atmos. Sci.*, **30**, 611–627.

Yang, J., B. Wang, B. Wang, and Q. Bao, 2010: Biweekly and 21–30-day variations of the subtropical summer monsoon rainfall over the lower reach of the Yangtze River basin. *J. Climate*, **23**, 1146–1160.

Accepted for publication in *Journal of Climate*. DOI10.1175/JCLI-D-19-0337.1.

Figure Captions

Fig. 1. SAT anomalies over the summer (JJA) of 2018 relative to the climatological JJA mean derived from the (a) ERA-Interim, (b) MERRA2 and (c) FNL datasets. The rectangle marks the area of Northeast Asia (32.5°−47.5°N, 110°−140°E) with significant warm anomalies. (d)–(f) Temporal evolutions of Northeast Asia area-averaged SAT in the climatological mean (black curve) and the anomalies (red and blue shading) in summer 2018 derived from the (d) ERA-Interim, (e) MERRA2 and (f) FNL datasets. Gray shading covers the period of Northeast Asian heatwave occurrence. Dots indicate the SAT anomalies exceed the 90th percentile. Units: °C.

Fig. 2. Geographical distributions of (a) 200-hPa and (c) 500-hPa geopotential height (shading; units: $m^2 s^{-2}$) in the summer (JJA) of 2018 and its anomaly (contours; units: $m^2 s^{-2}$) relative to the climatological mean of 1979–2018. The rectangle marks the area of Northeast Asia (32.5°−47.5°N, 110°−140°E) that experienced the heatwave in 2018. (b) and (d) Temporal evolutions of the Northeast Asia area-averaged geopotential height anomalies (bars; units: $m^2 s^{-2}$; left axis) at 200 and 500 hPa, respectively, during JJA 2018. The red curve represents the 30–90-day filtered geopotential height (units: $m^2 s^{-2}$; right axis). Gray shading covers the period of Northeast Asian heatwave occurrence.

Fig. 3. (a) 30–90-day filtered 500-hPa geopotential height (contours; units: $m^2 s^{-2}$) and SAT (shading; units: K) during the Northeast Asia heatwave period of 11 July to 14 August 2018. (b) 30–90-day temperature budget at 925 hPa over Northeast Asia during the heatwave period. From left to right: SAT tendency, horizontal advection, adiabatic heating associated with vertical motion and

Accepted for publication in *Journal of Climate*. DOI10.1175/JCLI-D-19-0337.1.

static stability, and diabatic heating. Units: 10^{-7} K s^{-1}. (c) As in (b) but for the surface energy budget terms. From left to right: surface net shortwave radiation, surface net thermal radiation, sensible heat flux, latent heat flux, and their summation. A positive (negative) value indicates an anomalous upward (downward) flux. Units: W m^{-2}.

Fig. 4. (a) MJO phase evolutions during the summer of 2018. Blue, red, green and orange colors indicate the periods of 1–10 July, 11–20 July, 21–31 July and 1–11 August 2018, respectively. (b) Composites of 30–90-day filtered OLR over the tropics during the Northeast Asian heatwave period of 11 July to 14 August 2018. Units: W m^{-2}.

Fig. 5. 30–90-day vorticity anomalies (shading; units: 10^{-6} s^{-1}) and WAF (vectors; units: m^2 s^{-2}) at the levels of (a) 850 hPa, (b) 500 hPa and (c) 200 hPa during the Northeast Asian heatwave period of 11 July to 14 August 2018. The black triangle marks the location of the enhanced MJO convective center.

Fig. 6. MJO phase composites of 30–90-day filtered OLR (shading; units: W m^{-2}) and 500-hPa geopotential height (contours; units: m) during the RMM phases (a) 1–2, (b) 3–4, (c) 5–6 and (d) 7–8 in JJA of 1979–2018. The active MJO days with the RMM amplitude greater than 1 were selected for the composite. The numbers of days for the composite are shown in the upper-right corners in parentheses. Only the anomalous fields statistically significant at the 95% confidence level relative to the climatological mean are shown. (e)–(h) As in (a)–(d) but for the composites based on the days with RMM amplitude greater than 1.5.

Accepted for publication in *Journal of Climate*. DOI10.1175/JCLI-D-19-0337.1.

Fig. 7. Temporal evolutions of 30–90-day SAT anomalies over Northeast Asia (32.5°–47.5°N, 110°–140°E) at (lag 0 day) and after (lag 1–14 days) the occurrence of RMM phases 5–6 based on the composites of days with RMM amplitude greater than (a) 1 and (b) 1.5, respectively. The *y*-axes on the left and right represent the 30–90-day SAT anomalies (units: K) and their normalized values (units: standard deviation), respectively. The numbers of days for the composite are shown in the upper-right corners in parentheses. (c)–(d) As in (a)–(b) but for the 30–90-day geopotential height anomalies (units: $m^2\,s^{-2}$) over Northeast Asia.

Fig. 8. (a) MJO phase indices during the occurrence of all Northeast Asian heatwave days during July–August from 1979 to 2018. (b) As in (a) but including the preceding periods (from 7 days ahead) of each heatwave day. The ratio of the numbers of heatwave days lying in each phase (excluding the days of weak MJO phase, RMM < 1) to the total number of heatwave days is shown in red at the corners. Asterisks indicate statistical significance at the 95% confidence level using the Monte Carlo method, in which random MJO phases were assigned to heatwave days for a large number of times (5000). If the probability of heatwave occurrence for a certain MJO phase is larger (smaller) than the 97.5% (2.5%) percentile of the random distribution generated by 5000 simulations, it is considered statistically significant.

Fig. 9. Left panels: Composites of 30–90-day OLR (units: W m^{-2}) based on the dates with enhanced western Pacific (0°–15°N, 100°–150°E) MJO convection in the (a) CTRL and (b) LP90 experiment. An enhanced MJO day was defined as when the normalized 30–90-day MJO-related convection was greater than one

Accepted for publication in *Journal of Climate*. DOI10.1175/JCLI-D-19-0337.1.

standard deviation over the western Pacific in the CTRL experiment. The same dates were used for the composite in the LP90 experiment, in which the MJO signals were removed artificially. The numbers of enhanced MJO days selected for the composite are shown in the upper-right corner in parentheses. (c) Composites of the 30–90-day SAT anomaly (units: K) over Northeast Asia (32.5°−47.5°N, 110°−140°E) from the CTRL (red bar) and LP90 (blue bar) experiment after 1−12 days of the occurrence of enhanced western Pacific MJO. Right panels: As in the left panels but for the composites based on the dates with stronger western Pacific MJO convections when the western Pacific-averaged 30–90-day OLR anomaly was greater than 1.5 standard deviations.

Fig. 10. (a) Composites of 30–90-day geopotential height anomaly at 500 hPa (units: m) after 1–12 days of the occurrence of enhanced western Pacific MJO (greater than one standard deviation) in EXP_CTRL. (b) As in (a) but for the composite results in EXP_LP90.

Fig. 11. Weekly mean SAT anomalies over Northeast Asia (32.5°–47.5°N, 110°–140°E) during the heatwave period (11 July to 14 August 2018) predicted by the (a) CMA and (b) JMA S2S models. Blue, red, green and orange curves indicate 1–4-week-lead predictions, respectively. Dots represent the ensemble mean, with the ensemble spread shown by vertical lines. The black curve indicates the weekly SAT evolutions derived from ERA-Interim. Units: K.

Fig. 12. Left panels: CMA S2S model predicted (a) MJO (RMM index), (b) SAT and (c) H500 anomalies over Northeast Asia (32.5°–47.5°N, 110°–140°E) for the heatwave period (11 July to 14 August 2018). Right panels: as in the left

Accepted for publication in *Journal of Climate*. DOI10.1175/JCLI-D-19-0337.1.

panels but for the JMA model predictions. The black curve represents the observed conditions during 11 July to 14 August 2018. Blue, red, green and orange curves present the forecasts started on 4 July (lead: 7–40 days), 27 June (lead: 14–54 days), 20 June (lead: 21–61 days) and 13 June (lead: 28–68 days), respectively. Dots represent the ensemble mean, with the ensemble spread shown by vertical lines.

Accepted for publication in *Journal of Climate*. DOI10.1175/JCLI-D-19-0337.1.

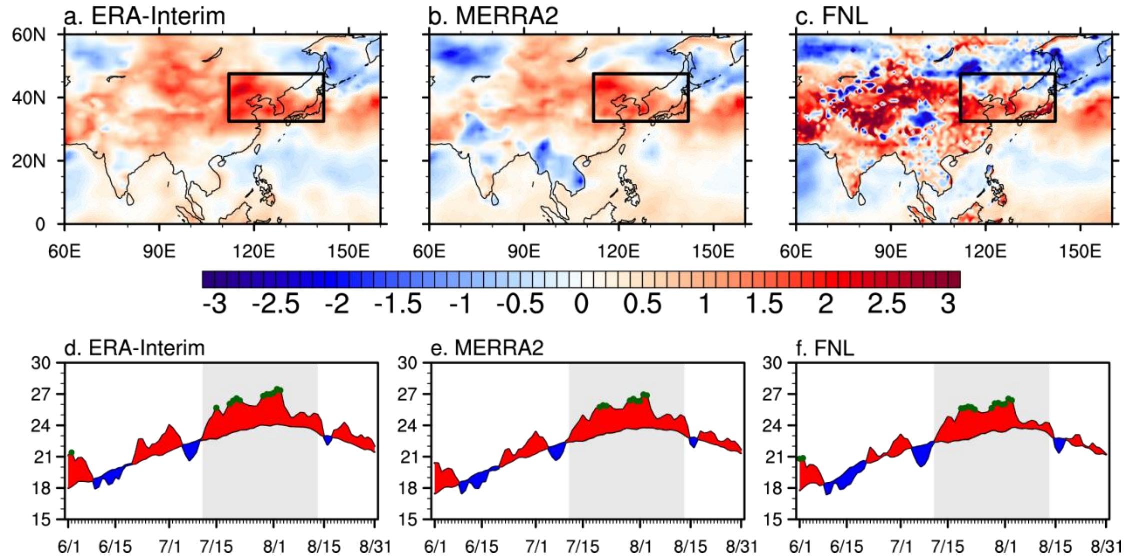

Fig. 1. SAT anomalies over the summer (JJA) of 2018 relative to the climatological JJA mean derived from the (a) ERA-Interim, (b) MERRA2 and (c) FNL datasets. The rectangle marks the area of Northeast Asia (32.5°–47.5°N, 110°–140°E) with significant warm anomalies. (d)–(f) Temporal evolutions of Northeast Asia area-averaged SAT in the climatological mean (black curve) and the anomalies (red and blue shading) in summer 2018 derived from the (d) ERA-Interim, (e) MERRA2 and (f) FNL datasets. Gray shading covers the period of Northeast Asian heatwave occurrence. Dots indicate the SAT anomalies exceed the 90th percentile. Units: °C.

Accepted for publication in *Journal of Climate*. DOI10.1175/JCLI-D-19-0337.1.

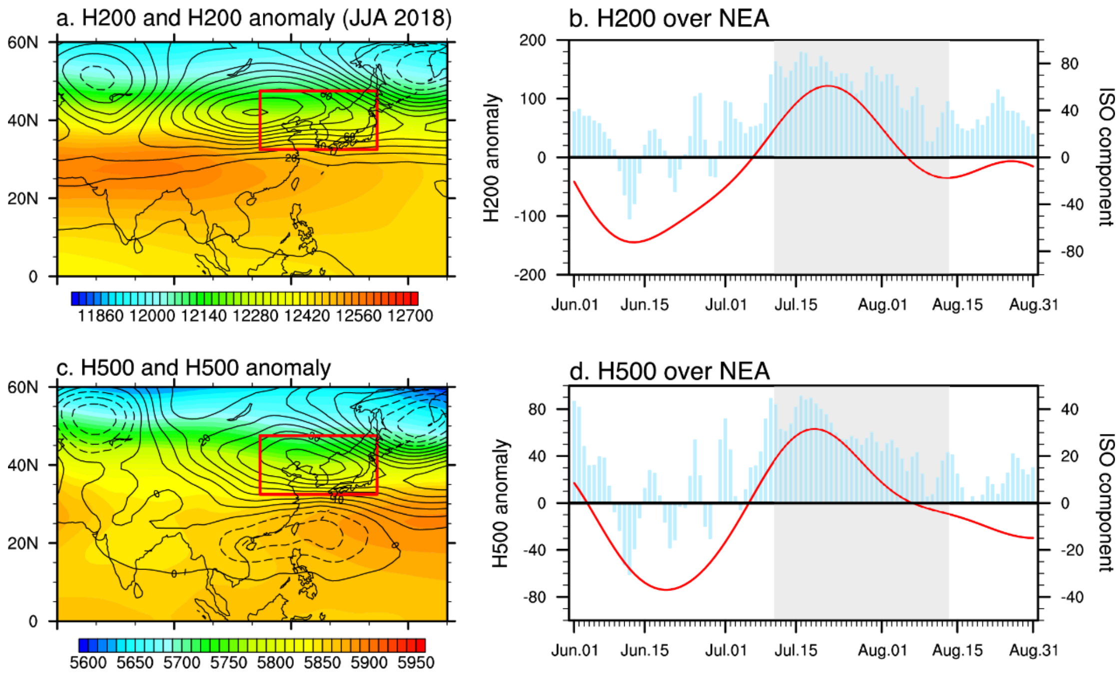

Fig. 2. Geographical distributions of (a) 200-hPa and (c) 500-hPa geopotential height (shading; units: $m^2 s^{-2}$) in the summer (JJA) of 2018 and its anomaly (contours; units: $m^2 s^{-2}$) relative to the climatological mean of 1979–2018. The rectangle marks the area of Northeast Asia (32.5°−47.5°N, 110°−140°E) that experienced the heatwave in 2018. (b) and (d) Temporal evolutions of the Northeast Asia area-averaged geopotential height anomalies (bars; units: $m^2 s^{-2}$; left axis) at 200 and 500 hPa, respectively, during JJA 2018. The red curve represents the 30–90-day filtered geopotential height (units: $m^2 s^{-2}$; right axis). Gray shading covers the period of Northeast Asian heatwave occurrence.

Accepted for publication in *Journal of Climate*. DOI 10.1175/JCLI-D-19-0337.1.

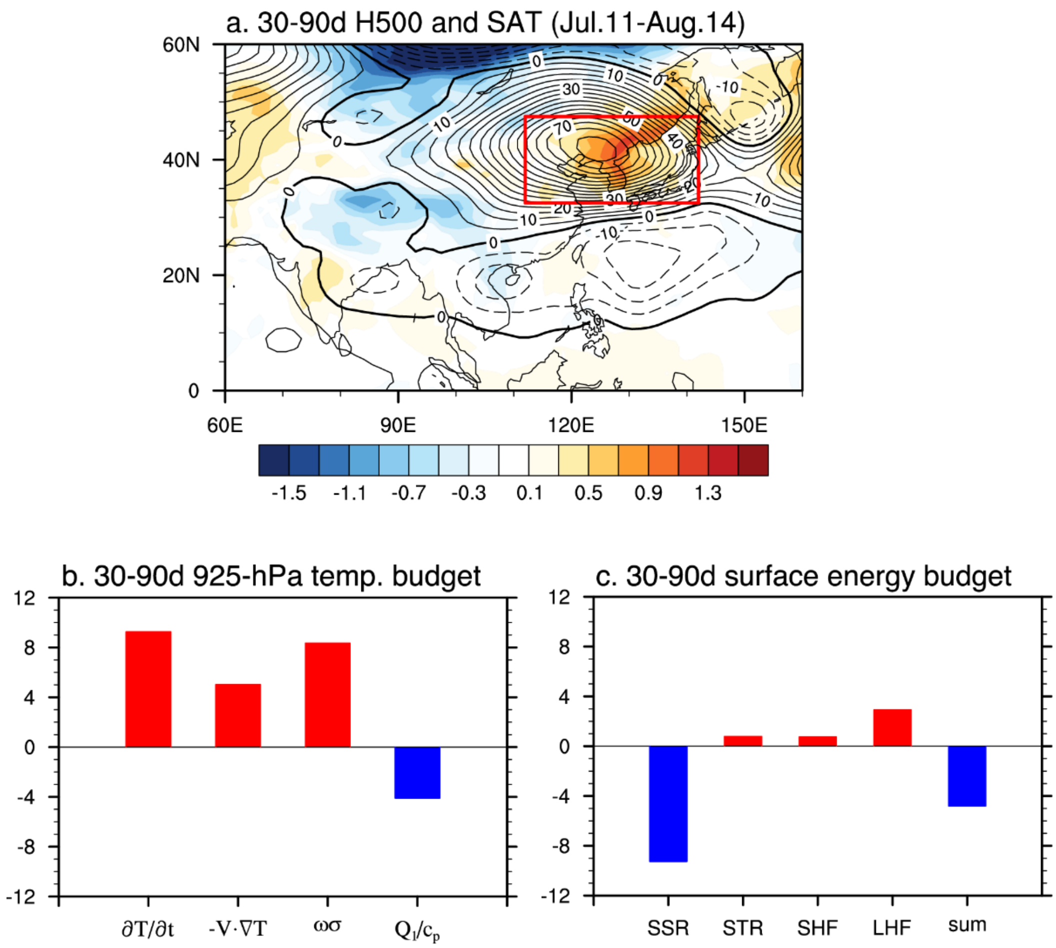

Fig. 3. (a) 30–90-day filtered 500-hPa geopotential height (contours; units: $m^2 s^{-2}$) and SAT (shading; units: K) during the Northeast Asia heatwave period of 11 July to 14 August 2018. (b) 30–90-day temperature budget at 925 hPa over Northeast Asia during the heatwave period. From left to right: SAT tendency, horizontal advection, adiabatic heating associated with vertical motion and static stability, and diabatic heating. Units: 10^{-7} K s^{-1}. (c) As in (b) but for the surface energy budget terms. From left to right: surface net shortwave radiation, surface net thermal radiation, sensible heat flux, latent heat flux, and their summation. A positive (negative) value indicates an anomalous upward (downward) flux. Units: W m^{-2}.

Accepted for publication in *Journal of Climate*. DOI10.1175/JCLI-D-19-0337.1.

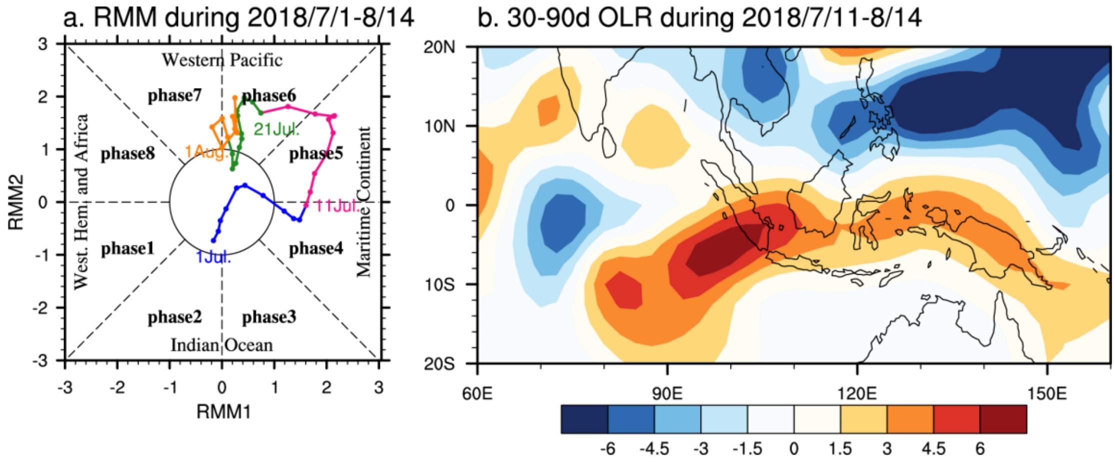

Fig. 4. (a) MJO phase evolutions during the summer of 2018. Blue, red, green and orange colors indicate the periods of 1–10 July, 11–20 July, 21–31 July and 1–11 August 2018, respectively. (b) Composites of 30–90-day filtered OLR over the tropics during the Northeast Asian heatwave period of 11 July to 14 August 2018. Units: W m^{-2}.

Accepted for publication in *Journal of Climate*. DOI10.1175/JCLI-D-19-0337.1.

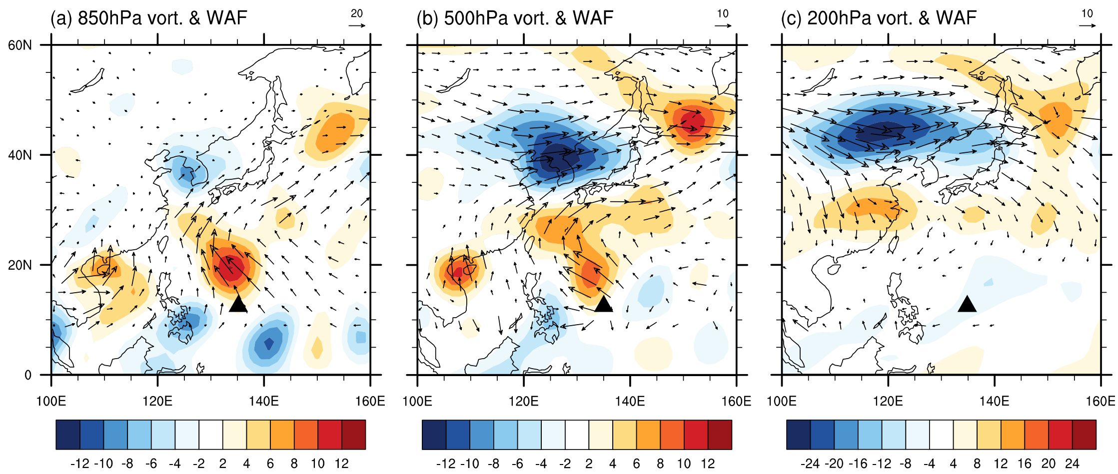

Fig. 5. 30–90-day vorticity anomalies (shading; units: 10^{-6} s^{-1}) and WAF (vectors; units: m^2 s^{-2}) at the levels of (a) 850 hPa, (b) 500 hPa and (c) 200 hPa during the Northeast Asian heatwave period of 11 July to 14 August 2018. The black triangle marks the location of the enhanced MJO convective center.

Accepted for publication in *Journal of Climate*. DOI10.1175/JCLI-D-19-0337.1.

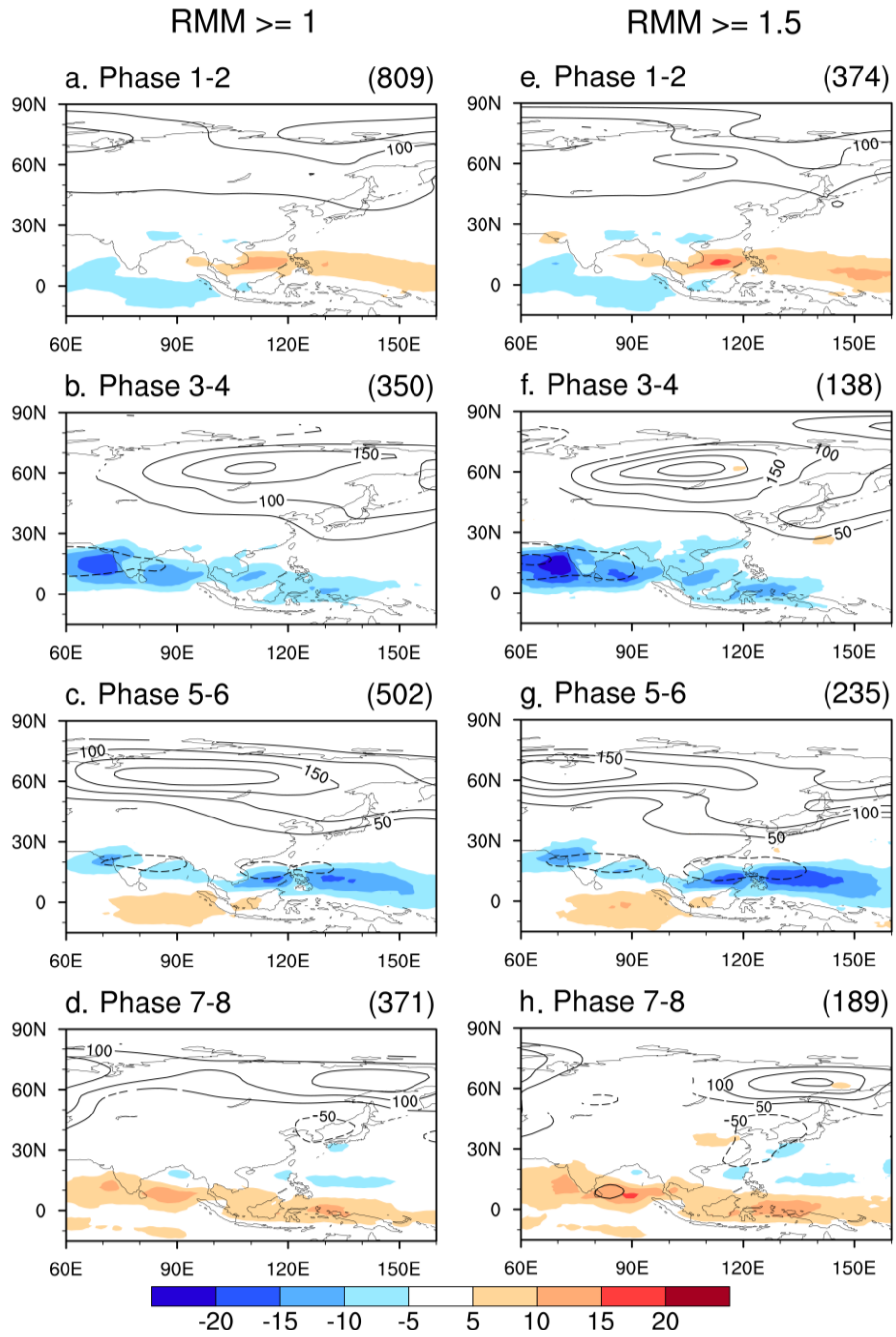

Fig. 6. MJO phase composites of 30–90-day filtered OLR (shading; units: W m^{-2}) and 500-hPa geopotential height (contours; units: m) during the RMM phases (a) 1–2, (b) 3–4, (c) 5–6 and (d) 7–8 in JJA of 1979–2018. The active MJO days with the RMM amplitude greater than 1 were selected for the composite. The numbers of days for the composite are shown in the upper-right corners in parentheses. Only the anomalous fields statistically significant at the 95% confidence level relative to the

Accepted for publication in *Journal of Climate*. DOI10.1175/JCLI-D-19-0337.1.

climatological mean are shown. (e)–(h) As in (a)–(d) but for the composites based on the days with RMM amplitude greater than 1.5.

Accepted for publication in *Journal of Climate*. DOI10.1175/JCLI-D-19-0337.1.

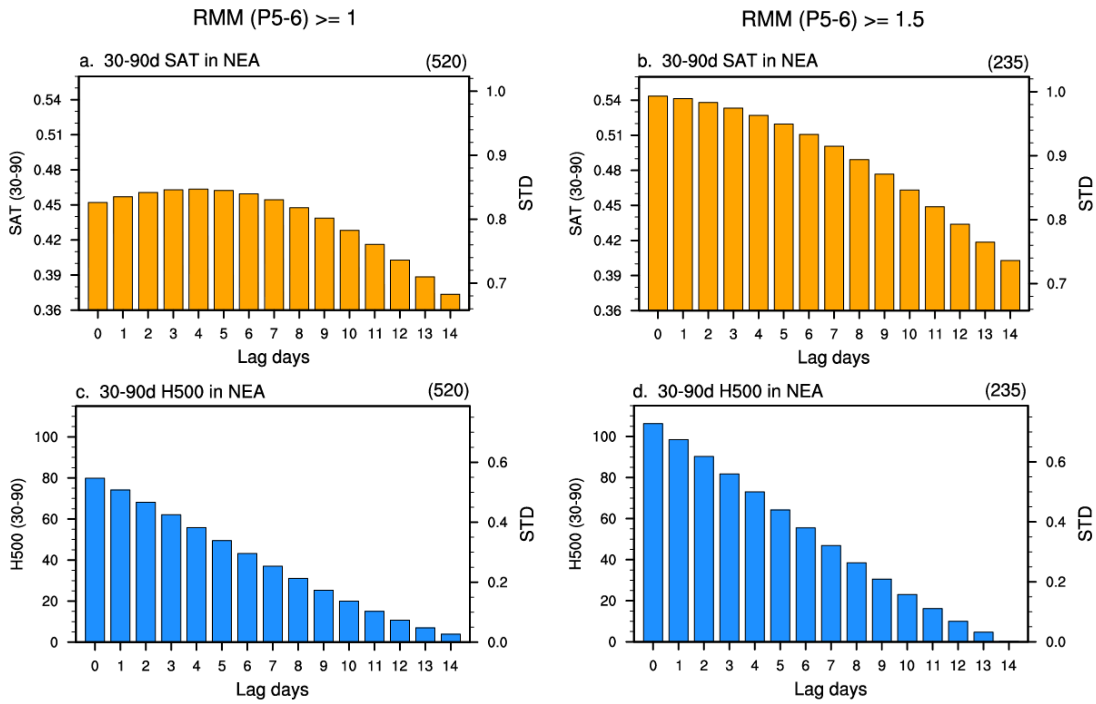

Fig. 7. Temporal evolutions of 30–90-day SAT anomalies over Northeast Asia (32.5°–47.5°N, 110°–140°E) at (lag 0 day) and after (lag 1–14 days) the occurrence of RMM phases 5–6 based on the composites of days with RMM amplitude greater than (a) 1 and (b) 1.5, respectively. The *y*-axes on the left and right represent the 30–90-day SAT anomalies (units: K) and their normalized values (units: standard deviation), respectively. The numbers of days for the composite are shown in the upper-right corners in parentheses. (c)–(d) As in (a)–(b) but for the 30–90-day geopotential height anomalies (units: $m^2\,s^{-2}$) over Northeast Asia.

Accepted for publication in *Journal of Climate*. DOI10.1175/JCLI-D-19-0337.1.

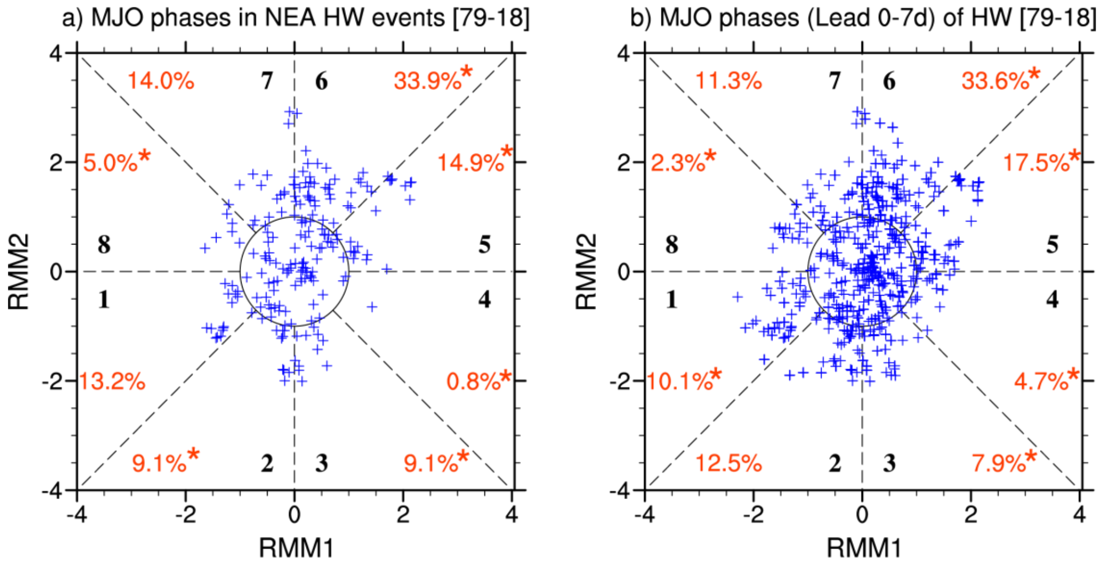

Fig. 8. (a) MJO phase indices during the occurrence of all Northeast Asian heatwave days during July–August from 1979 to 2018. (b) As in (a) but including the preceding periods (from 7 days ahead) of each heatwave day. The ratio of the numbers of heatwave days lying in each phase (excluding the days of weak MJO phase, RMM < 1) to the total number of heatwave days is shown in red at the corners. Asterisks indicate statistical significance at the 95% confidence level using the Monte Carlo method, in which random MJO phases were assigned to heatwave days for a large number of times (5000). If the probability of heatwave occurrence for a certain MJO phase is larger (smaller) than the 97.5% (2.5%) percentile of the random distribution generated by 5000 simulations, it is considered statistically significant.

Accepted for publication in *Journal of Climate*. DOI 10.1175/JCLI-D-19-0337.1.

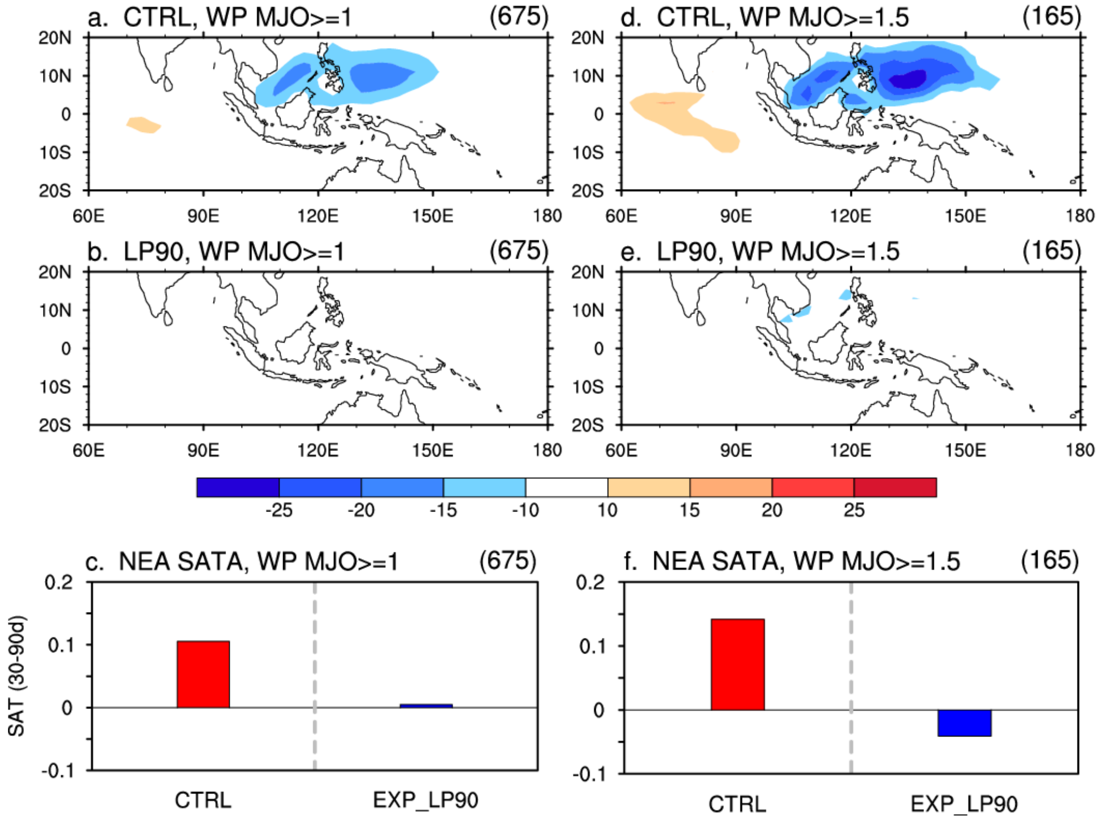

Fig. 9. Left panels: Composites of 30–90-day OLR (units: W m^{-2}) based on the dates with enhanced western Pacific (0°–15°N, 100°–150°E) MJO convection in the (a) CTRL and (b) LP90 experiment. An enhanced MJO day was defined as when the normalized 30–90-day MJO-related convection was greater than one standard deviation over the western Pacific in the CTRL experiment. The same dates were used for the composite in the LP90 experiment, in which the MJO signals were removed artificially. The numbers of enhanced MJO days selected for the composite are shown in the upper-right corner in parentheses. (c) Composites of the 30–90-day SAT anomaly (units: K) over Northeast Asia (32.5°–47.5°N, 110°–140°E) from the CTRL (red bar) and LP90 (blue bar) experiment after 1–12 days of the occurrence of enhanced western Pacific MJO. Right panels: As in the left panels but for the composites based on the dates with stronger western Pacific MJO convections when the western Pacific-averaged 30–90-day OLR anomaly was greater than 1.5 standard deviations.

Accepted for publication in *Journal of Climate*. DOI10.1175/JCLI-D-19-0337.1.

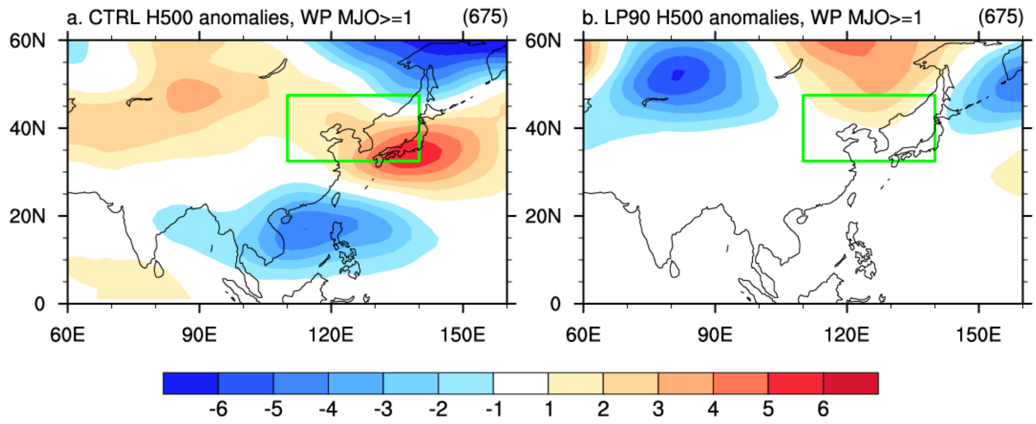

Fig. 10. (a) Composites of 30–90-day geopotential height anomaly at 500 hPa (units: m) after 1–12 days of the occurrence of enhanced western Pacific MJO (greater than one standard deviation) in EXP_CTRL. (b) As in (a) but for the composite results in EXP_LP90.

Accepted for publication in *Journal of Climate*. DOI10.1175/JCLI-D-19-0337.1.

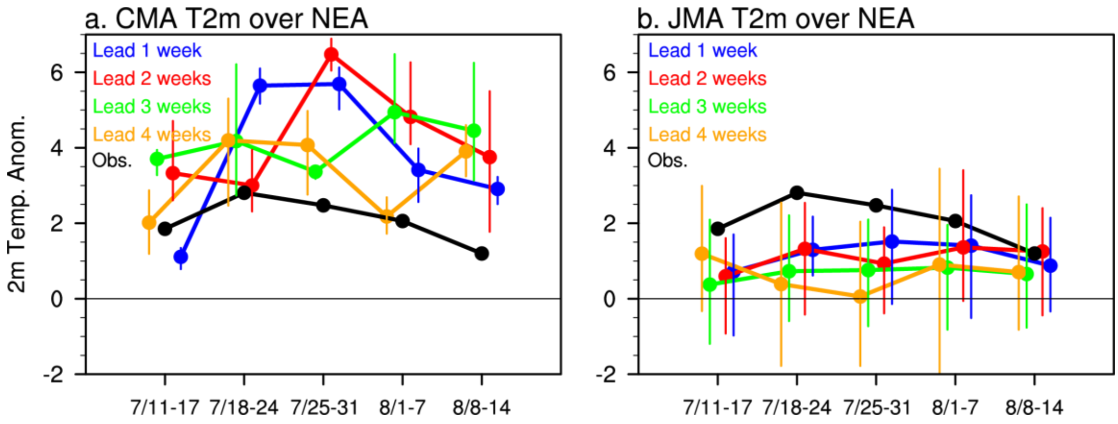

Fig. 11. Weekly mean SAT anomalies over Northeast Asia (32.5°–47.5°N, 110°–140°E) during the heatwave period (11 July to 14 August 2018) predicted by the (a) CMA and (b) JMA S2S models. Blue, red, green and orange curves indicate 1–4-week-lead predictions, respectively. Dots represent the ensemble mean, with the ensemble spread shown by vertical lines. The black curve indicates the weekly SAT evolutions derived from ERA-Interim. Units: K.

Accepted for publication in *Journal of Climate*. DOI 10.1175/JCLI-D-19-0337.1.

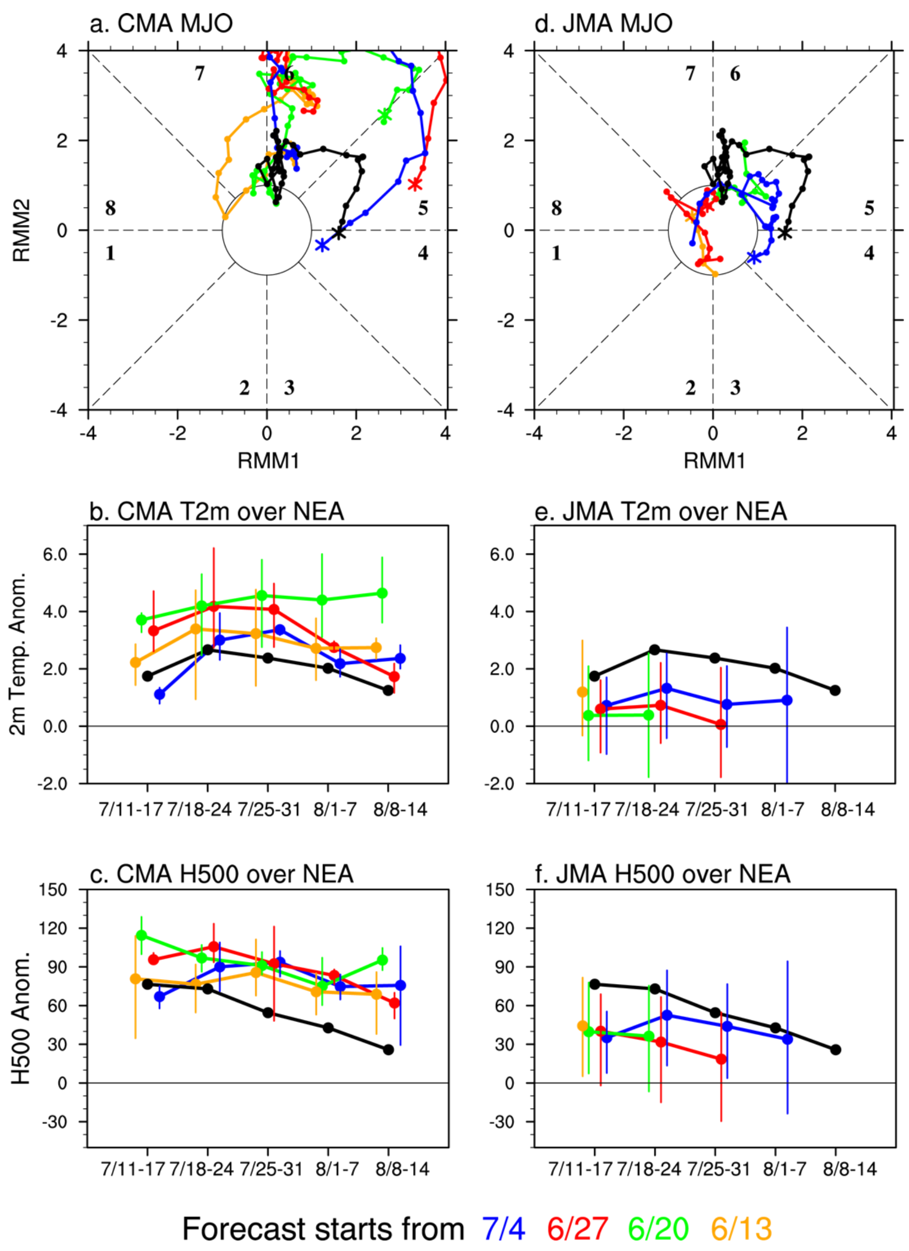

Fig. 12. Left panels: CMA S2S model predicted (a) MJO (RMM index), (b) SAT and (c) H500 anomalies over Northeast Asia (32.5°–47.5°N, 110°–140°E) for the heatwave period (11 July to 14 August 2018). Right panels: as in the left panels but for the JMA model predictions. The black curve represents the observed conditions during 11 July to 14 August 2018. Blue, red, green and orange curves present the forecasts started on 4 July (lead: 7–40 days), 27 June (lead: 14–54 days), 20 June (lead: 21–61 days) and 13 June (lead: 28–68 days), respectively. Dots represent the ensemble mean, with the ensemble spread shown by vertical lines.

Accepted for publication in *Journal of Climate*. DOI10.1175/JCLI-D-19-0337.1.